



**HAL**  
open science

# Shape dynamics of rotating polygons on the surface of liquid nitrogen in a Leidenfrost state

Jacob S. Bach, Alexis Duchesne, Tomas Bohr

► **To cite this version:**

Jacob S. Bach, Alexis Duchesne, Tomas Bohr. Shape dynamics of rotating polygons on the surface of liquid nitrogen in a Leidenfrost state. *Comptes Rendus. Mécanique*, 2020, 348 (6-7), pp.457-473. 10.5802/crmeca.24 . hal-03322812

**HAL Id: hal-03322812**

**<https://hal.science/hal-03322812>**

Submitted on 13 Jul 2022

**HAL** is a multi-disciplinary open access archive for the deposit and dissemination of scientific research documents, whether they are published or not. The documents may come from teaching and research institutions in France or abroad, or from public or private research centers.

L'archive ouverte pluridisciplinaire **HAL**, est destinée au dépôt et à la diffusion de documents scientifiques de niveau recherche, publiés ou non, émanant des établissements d'enseignement et de recherche français ou étrangers, des laboratoires publics ou privés.



Distributed under a Creative Commons Attribution 4.0 International License



INSTITUT DE FRANCE  
Académie des sciences

# *Comptes Rendus*

---

## *Mécanique*

Jacob S. Bach, Alexis Duchesne and Tomas Bohr

**Shape dynamics of rotating polygons on the surface of liquid nitrogen in a Leidenfrost state**


Volume 348, issue 6-7 (2020), p. 457-473.

<<https://doi.org/10.5802/crmeca.24>>

**Part of the Thematic Issue:** Tribute to an exemplary man: Yves Couder

**Guest editors:** Martine Ben Amar (Paris Sciences & Lettres, LPENS, Paris, France), Laurent Limat (Paris-Diderot University, CNRS, MSC, Paris, France), Olivier Pouliquen (Aix-Marseille Université, CNRS, IUSTI, Marseille, France) and Emmanuel Villermaux (Aix-Marseille Université, CNRS, Centrale Marseille, IRPHE, Marseille, France)

© Académie des sciences, Paris and the authors, 2020.  
*Some rights reserved.*

 This article is licensed under the  
CREATIVE COMMONS ATTRIBUTION 4.0 INTERNATIONAL LICENSE.  
<http://creativecommons.org/licenses/by/4.0/>



*Les Comptes Rendus. Mécanique sont membres du  
Centre Mersenne pour l'édition scientifique ouverte*  
[www.centre-mersenne.org](http://www.centre-mersenne.org)



---

Tribute to an exemplary man: Yves Couder

Instabilities, patterns

# Shape dynamics of rotating polygons on the surface of liquid nitrogen in a Leidenfrost state

Jacob S. Bach<sup>a</sup>, Alexis Duchesne<sup>a, b</sup> and Tomas Bohr<sup>\*, a</sup>

<sup>a</sup> Department of Physics, Technical University of Denmark, DK-2800 Kgs. Lyngby, Denmark

<sup>b</sup> Université de Lille, CNRS, UMR 8520-IEMN, Avenue Poincaré, 59652 Villeneuve d'Ascq, France

*E-mails:* [jasoba@fysik.dtu.dk](mailto:jasoba@fysik.dtu.dk) (J. S. Bach), [alexis.duchesne@univ-lille.fr](mailto:alexis.duchesne@univ-lille.fr) (A. Duchesne), [tbohr@fysik.dtu.dk](mailto:tbohr@fysik.dtu.dk) (T. Bohr)

**Abstract.** When liquid nitrogen is set into rotation in a warm pot, the surface, initially forming an axis-symmetrical, toroidal shape, spontaneously re-structures into a series of rotating polygons with a diminishing number of corners, while slowing down. This spontaneous “ordering” occurs despite the violently turbulent and boiling state of the fluid. We show experimentally that these shapes are well-described as a sum of a few Fourier modes, and we present experimental results for the development of the frequencies and amplitudes of these wave-modes during the transient process. We compare our results with the theoretical results for the instabilities of a potential vortex flow and argue that the first polygon formed in the transient process should be described by this theory. The paper is dedicated to the memory of Yves Couder, colleague, friend and a life-long source of inspiration.

**Résumé.** Dans cet article nous nous intéressons au cas d'un volume d'azote liquide en état de caléfaction mis en rotation dans un récipient cylindrique chauffé. La surface libre du liquide, initialement sous forme d'un tore axisymétrique, va se déstabiliser et se restructurer en une série de polygones tournants dont le nombre de côtés diminue à mesure que le liquide ralentit. Ce facettage apparaît spontanément alors même que le liquide connaît une violente ébullition et un écoulement extrêmement turbulent. Nous démontrons expérimentalement que les formes observées peuvent être décrites par la combinaison d'un petit nombre de modes de Fourier et nous étudions l'évolution de ces modes en termes d'amplitude et de fréquence depuis le premier polygone visible jusqu'à la fin de la rotation du liquide. Nous comparons nos résultats expérimentaux avec un modèle théorique décrivant la perte de stabilité des écoulements de type vortex potentiel et nous soutenons que le premier polygone observable suite à la déstabilisation de la forme axisymétrique peut être décrit par ce modèle. Cet article est dédié à la mémoire d'Yves Couder qui fut pour nous un collègue, un ami et une intarissable source d'inspiration.

**Keywords.** Rotating polygons, Fluid instabilities, Free surface flows, Spontaneous symmetry breaking, Shape dynamics.

---

\* Corresponding author.

## 1. Introduction by Tomas Bohr

Yves Couder was a pioneer in the field of pattern formation that emerged through the 1980's from nonlinear dynamics, chaos, statistical mechanics and fluid mechanics. His background included condensed matter physics, and electronic band structures and his first work was on cyclotron resonance and Landau levels in very pure Tellurium – a single author paper in *Physical Review Letters* [1]. So when, late in his career, he discussed “Landau levels” formed by walking droplets on a vibrating, rotating table [2], he knew what he was talking about. For him, the change of field came around 1980, when he started his work on classical systems and instabilities by looking at soap films [3], an experimental system that followed him for many years and that he managed to turn into a surprising and efficient laboratory for the study of 2-D fluid dynamics.

I met him for the first time at the Cargèse summer school “New Trends in Nonlinear Dynamics and Pattern-Forming Phenomena” in 1988 and again at that same beautiful place in “Growth and Form” in 1990. At that time Yves was already a well-established leader of the field, attracting brilliant students and co-workers. I remember the impression, at these first encounters, of the originality, quality and clarity of Couder's work. At that time he was trying to understand viscous fingering, and I remember my surprise that one could solve (or reproduce) the result that the limiting stable viscous finger has the width of half the channel in the presence of surface tension – a strongly nonlinear fluid dynamics problem – by looking at the statistical physics of random walkers [4]. Both the style of Couder's work and the style of the schools themselves made a deep impression on me and inspired me to organize summer schools in Denmark as well. This became the series “Complex Motion in Fluids”, where Yves lectured himself in 2011, as testified in Figure 1. The encounters with Yves also gave me courage and inspiration to introduce experimental work on fluids in my own research.

In 2003, I was asked to advise on plans for the new MSC lab at Paris 7, and I had many discussions with Yves on that issue. He was very enthusiastic about the prospects of the new lab, but he was reluctant to leave his beloved LPS at École Normale Supérieure. Seeing his beautiful and productive lab in the finished MSC lab some years later, with direct access to the scenic roof of the building, made me sure that he made the right decision! He also showed me his impressive collection of leaves and their images for his studies of venation structures of plant leaves [5,6] and his work on this subject, including the effects of stress on plant growth [7], definitely contributed to my own choice of studying flows in plants [8]. Several times, he urged me to study algae. Unfortunately, I did not follow this admonition in time to get his advice, but it is still on my agenda! My own first hydrodynamical experiment was on hydraulic jumps. In Denmark such a subject, which reminded of a kitchen sink, was not considered “fundamental physics”. People would smile politely and then ask what on earth it might be useful for. Quite opposite, Yves was very interested and asked penetrating questions, on both theory and experiments. In 2009, when I visited the MSC lab, I was asked to give three (long) lectures on hydraulic jumps – and Yves was there the whole time! He even showed me that he could very simply reproduce our polygonal hydraulic jumps by inserting a ring at some distance from the jet.

In 2012 he co-authored a very interesting paper [9] studying large Leidenfrost “drops”: levitating Leidenfrost tori made by pouring water into a hot circular metal trough. This system is well suited for studying hydrodynamical instabilities of surface waves, akin to those seen in hydraulic jumps, but which are considerably harder to do in a clean way in the hydraulic jump case due to the no-slip condition on the solid substrate. At roughly the same time, we also introduced large Leidenfrost “drops” in our experiments, the subject of the present paper. They are even larger than those investigated by Couder *et al.* – around one liter – and instead of using water, we use liquid nitrogen set into rotation in a warm pot.



**Figure 1.** Group picture from the summer school *Complex Motion in Fluids* at Krogerup Højskole in August 2011, where Yves Couder (fourth standing person from the left) gave two seminal lectures on “Classical wave particle duality”.

Our motivation for these experiments came from some of our earlier papers, actually referenced by Couder *et al.* as an application of their Leidenfrost tori. Here they mention the polygonal hydraulic jumps [10], where one side of the jump deforms to something looking almost identical to the polygonal tori. But they also mention “instabilities in partially filled tanks” [11–13], the subject of the present paper; and they pose as an open question, whether the polygons seen in those two very different systems have the same origin. In fact, we do not believe that they are much related: the polygonal hydraulic jumps are seen at intermediary Reynolds numbers – of the order of  $10^2$  or less – and are believed to be caused by surface tension [14, 15], while “rotating polygons” seen on swirling flows have Reynolds numbers in the  $10^5$ -regime, and are believed to be caused by wave resonances [16, 17], as we shall describe in the present paper.

## 2. Rotating polygons and wave resonances

The experiments showing “rotating polygons” were initially done by submitting a cylindrical tank, partially filled with water, to rotation; but only by rotating the bottom, not the cylinder itself, which remains stationary. This is illustrated in Figure 2, where the left side (a) shows the so-called “Newton’s bucket” flow – the flow in a bucket rotating with constant speed, where the flow comes to rest in the rotating frame, and where the parabolic free surface shows that this frame is not inertial. On the right hand side (b), only the bottom of the cylinder is rotating, so there is no rotating frame in which the flow can come to rest. The difference between the surface shapes in the two cases is marked: The water in the rigidly rotating case (a) occupies a concave region, whereas it is convex in the “frustrated” (b) case. And in contrast to the stable case (a) the frustrated flow can be unstable and spontaneously deform in to a rotating wave – what we call a

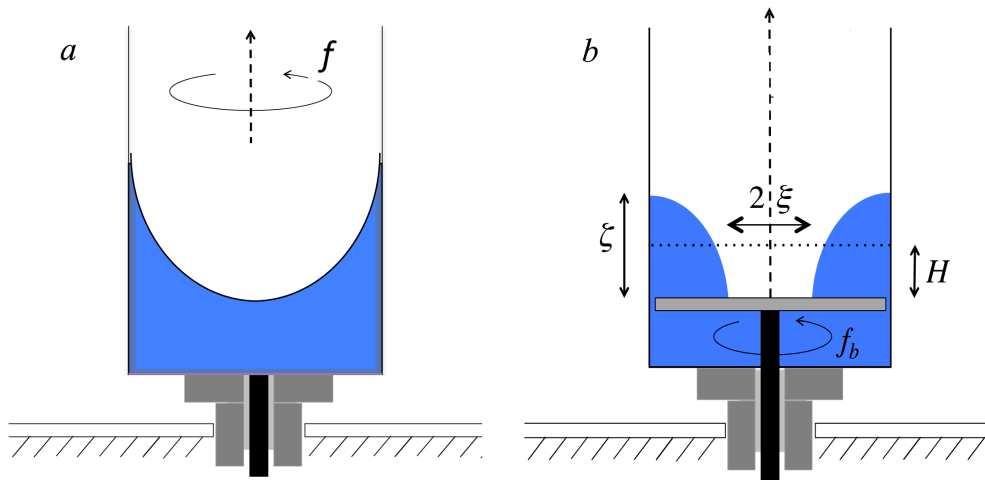


**Figure 2.** Two different rotating flows. In the “happy” Newton’s bucket flow (a), the whole system is rotating, and the system comes to rest in the rotating frame. In the “frustrated” bucket (b), only the bottom is rotated (with frequency  $\omega = 2\pi f_b$ ) so there is no rotating frame, where the flow can come to rest. In addition to the rapid azimuthal flow there is a small (secondary) radial component. It was argued in [13] and [20] that it should be close to a potential vortex flow.

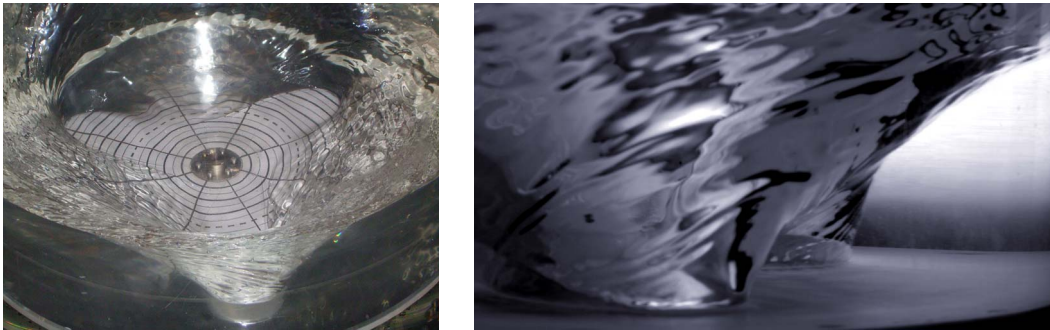


**Figure 3.** A rotating triangle in water. (a) From above. (b) From the side. Courtesy of Barbara Bohr.

“rotating polygon” – with up to six corners [18, 19]. Figure 3 shows a rotating “triangle”. As one can see the surface deformations can be rather large and dramatic! The polygons shown in Figure 3 have been called “dry” [12] since the centrifugal forces are large enough to create a dry hole in the middle of the plate. One also finds “wet” states where the free surface never touches the bottom plate. In the following, we shall only discuss the dry states.

The first papers describing this instability [11, 12] contained no theoretical explanation. It was much later [16] that a theory was presented. The first step was taken in [13], where it was noted that the polygonal structures developed via an axially symmetric, circular state, which would then be a candidate for stability analysis. The question was then what the flow in this symmetric state looked like. This was answered by Laust Tophøj, who was working on his phd under the guidance of Tomas Bohr, trying to understand the general restrictions for motion on a free surface with an arbitrary but specified shape. The conclusion was [13, 20] that such an axially symmetric flow had

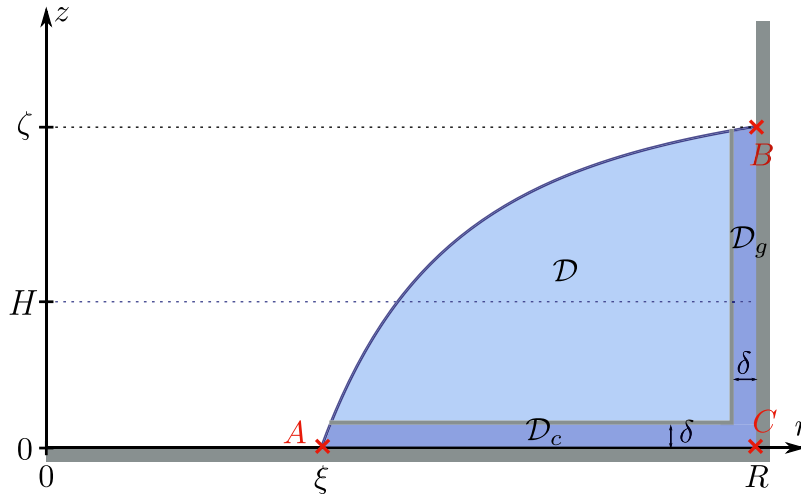


**Figure 4.** The “Tophøj” model. In stead of treating the entire surface, the attention is restricted to two regions: near the center and near the rim, respectively. These surface regions,  $A$  and  $B$  are coupled through the channels  $\mathcal{D}_c$  and  $\mathcal{D}_g$  and give rise to two families of excitations: *centrifugal*- and *gravitational* waves, respectively [16].

to have the form of a *line vortex*, except in the special situation where the radial flow vanished – as e.g., the Newton’s bucket flow Figure 2a. Simultaneously, Jerome Mougel was working for his phd under the guidance of David Fabre in Toulouse to understand instabilities of free surface, both analytically and numerically – in particular the Newton’s bucket flow [21]. When we told them that our base flow was probably a line vortex flow, they quickly showed numerically that such flows are actually unstable, and that the spectrum splits nicely into “families” living near the center and near the cylinder wall, respectively, as explained in detail in [17]. The theory in [16] was mostly focused on a simpler model, the “Tophøj” or “channel” model, replacing the analysis of the entire surface with narrow connected channels as shown in Figure 4 and thus utilizing the family-structure of the spectrum.

The line vortex flow is a potential, purely azimuthal, flow with velocity field

$$U(r) = \frac{\Gamma}{2\pi r} \tag{1}$$

where  $\Gamma$  is the circulation, and for an inviscid flow (neglecting surface tension) the shape of the free surface extending from the outer cylindrical wall of the system  $r = R$  to an inner radius  $\xi$  is

$$z_0(r) = \frac{1}{2g} \left( \frac{\Gamma}{2\pi R} \right)^2 \left( \frac{R^2}{\xi^2} - \frac{R^2}{r^2} \right) \tag{2}$$

and the outer height, which is  $H$  for the nonrotating system, is  $\zeta = z_0(R)$ . Correspondingly the volume of fluid  $V = 2\pi R^2 H$  is given

$$V = 2\pi \int_{\xi}^R z_0(r) r \, dr = \frac{\Gamma^2}{4\pi g} \left( \frac{R^2 - \xi^2}{2\xi^2} + \ln \left( \frac{\xi}{R} \right) \right). \tag{3}$$

The result of the stability analysis of the Tophøj model is a dispersion relation linking frequency  $\omega$  and wave number  $m$ , where  $m$  is the number of corners in the emerging polygon, and thus a positive integer. In the Tophøj model there are two channels:  $\mathcal{D}_g$ , where the surface is nearly horizontal and the restoring force is predominantly gravitational, and  $\mathcal{D}_c$ , where the surface is almost vertical and the restoring force is predominantly centrifugal. These channels



give rise to two “free wave” families – each containing a forward (compared to the current) and a backward moving wave with dispersion

$$D_g(\omega) = (\omega - m\Omega_R)^2 - gmF/R = 0 \quad (4)$$

$$D_c(\omega) = (\omega - m\Omega_\xi)^2 - g_c mF/\xi = 0 \quad (5)$$

where  $g$  is the gravitational acceleration,

$$g_c = \frac{U^2(\xi)}{\xi} = \frac{\Gamma^2}{4\pi^2 \xi^3} \quad (6)$$

is the centrifugal acceleration, and where  $\Omega_\xi = U(\xi)/\xi$  and  $\Omega_R = U(R)/R$  are the angular flow speeds in the two channels. Further

$$F = \frac{1 + e^{-2m\tilde{\zeta}} (\tilde{\xi})^{2m}}{1 - e^{-2m\tilde{\zeta}} (\tilde{\xi})^{2m}} \quad (7)$$

where  $\tilde{\zeta} = \zeta/R$  and  $\tilde{\xi} = \xi/R$ . Thus the free waves have dispersion

$$\omega_g^\pm = m\Omega_R \pm \sqrt{gmF/R} \quad (8)$$

$$\omega_c^\pm = m\Omega_\xi \pm \sqrt{g_c mF/\xi}. \quad (9)$$

With this notation, the dispersion relation for the full model of interacting waves can be written [16]

$$D_c(\omega)D_g(\omega) = \frac{mg}{R} \frac{mg_c}{\xi} (F^2 - 1). \quad (10)$$

Using

$$\tilde{V} = \frac{V}{\pi R^3} = \frac{H}{R}; \quad \tilde{\Gamma} = \frac{\Gamma}{2\pi\sqrt{gR^3}}; \quad \tilde{\omega} = \frac{\omega}{\sqrt{g/R}} \quad (11)$$

we can write

$$g_c = \frac{\tilde{\Gamma}^2}{\tilde{\xi}^3} g \quad (12)$$

and express

$$D_g(\omega) = \frac{g}{R} [(\tilde{\omega} - m\tilde{\Gamma})^2 - mF] \quad (13)$$

$$D_c(\omega) = \frac{g}{R} [(\tilde{\omega} - m\tilde{\Gamma}/\tilde{\xi}^2)^2 - m\tilde{\Gamma}F/\tilde{\xi}^4] \quad (14)$$

and, similarly, using (3), the scaled volume is

$$\tilde{V} = \tilde{\Gamma}^2 \left( \frac{1 - \tilde{\xi}^2}{2\tilde{\xi}^2} + \ln(\tilde{\xi}) \right) \quad (15)$$

and the scaled fluid height at the rim is

$$\tilde{\zeta} = \frac{1}{2} \tilde{\Gamma}^2 (\tilde{\xi}^{-2} - 1) \quad (16)$$

and we see that the dispersion relation is universal in the scaled variables, and that the knowledge of  $m$ ,  $\tilde{\xi}$  and  $\tilde{V}$  (or  $\tilde{\Gamma}$ ) completely specifies  $\tilde{\omega}$ . The scaled free waves are given by

$$\tilde{\omega}_g^\pm = m\tilde{\Gamma} \pm \sqrt{mF} \quad (17)$$

$$\tilde{\omega}_c^\pm = m\tilde{\Gamma}/\tilde{\xi}^2 \pm \sqrt{m\tilde{\Gamma}F/\tilde{\xi}^4} = \tilde{\xi}^{-2} (m\tilde{\Gamma} \pm \sqrt{m\tilde{\Gamma}F}). \quad (18)$$

In the scaled variables, the full dispersion (10) now becomes

$$((\tilde{\omega} - m\tilde{\Gamma})^2 - mF) ((\tilde{\omega} - m\tilde{\Gamma}\tilde{\xi}^{-2})^2 - m\tilde{\Gamma}^2 F \tilde{\xi}^{-4}) = m^2 \tilde{\Gamma}^2 \tilde{\xi}^{-4} (F^2 - 1) \quad (19)$$



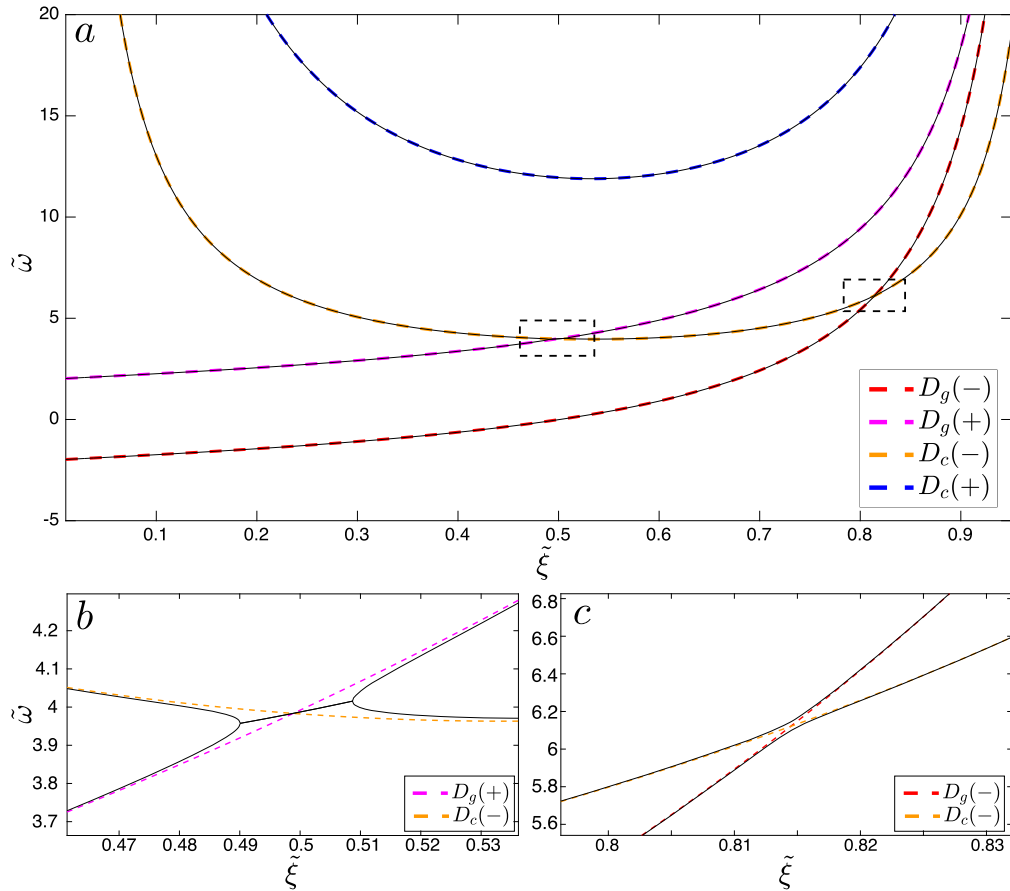


**Figure 5.** Real part of the frequency spectrum with level crossings and instabilities in the “Tophøj” model with  $\tilde{V} = 0.2$  and  $m = 4$ . The dashed lines represent the non-interacting waves, i.e. the solution of (17)–(18): forward gravitational (purple dashed), backward gravitational (red dashed), forward centrifugal (blue dashed) and backward centrifugal (yellow dashed), and the full lines show  $\Re[\tilde{\omega}]$  for the interacting system (10). Note that the dashed and the full lines are almost on top of each other except at the places where the different wave frequencies cross. (b) Blow-up of the crossing of a backward centrifugal wave and a forward gravitational wave giving rise to an instability in the interval  $(0.49 < \tilde{\xi} < 0.51)$ . Here  $\tilde{\omega}$  is complex and the system is linearly unstable. (c) Blow-up of the crossing of a backward centrifugal wave and a backward gravitational wave. The interacting waves (full line) “repel” each other and never cross, but exchange identity at the crossing of the non-interacting waves.

and the solution for  $\tilde{\omega}(\tilde{\xi})$  or, more correctly, the real part of  $\tilde{\omega}$ , is shown in Figure 5a for the case  $\tilde{V} = 0.2$  and  $m = 4$ . Here we clearly see the four waves: forward gravitational, backward gravitational, forward centrifugal and backward centrifugal waves. The dashed lines represent the non-interacting waves, i.e. the solution of (17)–(18), and the full lines show the interacting system (10). Note that the dashed and the full lines are almost on top of each other except at the places where the different wave frequencies cross, and this is due to the smallness of the (positive) factor  $F^2 - 1$ . The wave crossings are of two types: at the center a forward gravitation wave crosses a backward centrifugal one, and towards the right a backward gravitation wave

crosses a backward centrifugal one. On the blow-ups one can see that only the first type of crossing actually creates an instability (Figure 5(b)), whereas the two waves, in the second case, “repel” each other and actually never cross, but exchange identity at the crossing (Figure 5(c)). In the first case, there is an interval in  $\tilde{\xi}$  where  $\tilde{\omega}$  is complex and the real part has collapsed to a single value and this represents a true instability with exponential growth. This scenario is in agreement with Cairns [22] study of the Kelvin–Helmholtz instability, and it is interesting that, in the final state, the gravitational wave is completely dominated by the large centrifugal wave, which is a retrograde wave in a supercritical region and thus has “negative energy”.

As shown in [16] the predictions of the model compare reasonably well with experiments. The main difference is that the theory predicts rather thin regions of instability, whereas the experiments show that the polygon states basically fill up a whole compact phase space region. One reason for this is that the instabilities found in [16] are all *supercritical* in the sense that infinitesimal perturbation of the circular state leads to instability. Experimentally, this is probably not the case and it is known that the system displays a considerable amount of multistability [19]. For further analysis of the available experimental data, see [23]. Also, the “Tophøj” model has been used for the description of “surface switching” in [24] and the physics of the interacting waves has been studied in [25].

### 3. Polygons on a liquid nitrogen surface

The theoretical model described above, being inviscid, even potential does not take into account that the flow is set up by a rotating bottom. Also, it is impossible to design a rotating bottom which is perfectly horizontal and rotates without any wobbling. There then always remains a slight suspicion that these instabilities are triggered by the wobbling of the plate, although it has been demonstrated with care that the frequency of the rotating polygon and that of the bottom plate are not locked [19]. We were thus very happy that we were able to find similar instabilities in systems that are not rotating at all [16], relying on the Leidenfrost effect, where boiling creates a thin vapor layer that separates the liquid from the pot making the friction very small. If we pour liquid nitrogen into a heated cylindrical pot and set the nitrogen into rotation, either by stirring, or, as shown in Figure 6, by accelerating it down a ramp, it can rotate sufficiently long for spontaneous symmetry breaking to occur as seen in Figure 7 (from *Gallery of Fluid Motion*, 2018 [26]). Surprisingly, one can find very well-defined polygonal shapes (ranging from ellipses to hexagons) despite the transient and strongly turbulent nature of the flow. Of course, the polygons seen in the nitrogen experiment are not fixed: the number of corners will slowly decay, disappearing one by one, as discussed in detail later.

As sketched in Figure 6 the Liquid nitrogen (at 77 K) is filled in the loading chamber and after releasing the hatch it flows down through the pipe and into the pot. To find the volume, we measure the weight and capture a video of the flow during the experiment, and to make the correspondence, we need the density of liquid nitrogen which is typically given as  $\rho = 804 \text{ kg}\cdot\text{m}^{-3}$ . However, under the conditions of our experiment, where the nitrogen is poured into a pot of 60 °C and is strongly boiling, we found a density of  $\rho = 675 \text{ kg}\cdot\text{m}^{-3}$  for the stationary liquid nitrogen, and used that density also for obtaining the volume of the rotating fluid.

Two cold spotlights were needed to get enough light for the very short shutter time in the camera. The field of view of the camera also captured the weight display which gave perfect synchronization between the flow image and the weight. The spotlights were covered with a thin paper such that no sharp shadows were cast. We found it very important for the image analysis of the weight to have a very evenly distributed light over the display such that the only gradients were due to display contrast. In Table 1 we list the important information describing the experiment.

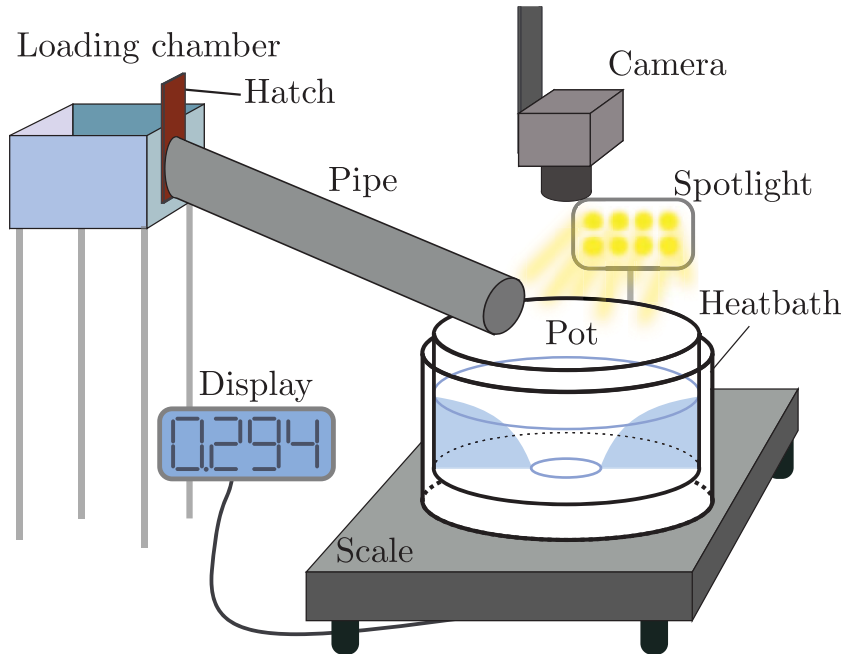


**Figure 6.** Experimental setup for the liquid nitrogen experiment. Liquid nitrogen is poured into the loading chamber with the hatch closed. When the hatch is lifted the liquid runs down the inclined pipe into one side of the pot of radius  $R = 10$  cm, kept at  $60^\circ\text{C}$  by the heat bath, ensuring a sufficient amount of angular momentum to keep the liquid rotating for around 1 min. After the liquid has been set into motion, a lid is mounted on top of the pot, allowing the evaporating nitrogen to expel the vapour and thus giving good visibility of the rotating liquid. The experimental data consist of videos of the liquid taken from above, allowing us to compute the distance  $\xi(\theta)$  from the center of the pot to the inner surface of the liquid as function of the angle, while simultaneously monitoring the mass (volume) of the liquid from the display of the scale.

### 3.1. Polygon shapes and their dynamics

As mentioned above, we concentrate on the “dry” polygons, where a part of the bottom of the pot is dry. In that case, it is easy to visualize the polygons, as was done for the water case by Bergmann *et al.* [13]. Using digital video-recordings we find the distance  $\xi(\theta)$  from the center of the pot to the inner nitrogen surface as function of the angle. This signal was decomposed into a Fourier series,

$$\xi(\theta, t) = \sum_{m=0}^M a_m(t) \cos(m\theta) + b_m(t) \sin(m\theta). \quad (20)$$

This can also be written terms of modes travelling with frequencies  $\omega_m$

$$\xi(\theta, t) = \sum_{m=0}^M A_m(t) \sin(m\theta - \omega_m t) \quad (21)$$

where

$$A_m(t) = \sqrt{a_m^2(t) + b_m^2(t)}, \quad \omega_m t = -\tan^{-1}(a_m(t)/b_m(t)). \quad (22)$$

To be meaningful,  $A_m$  and  $\omega_m$  should be varying slowly in time compared to  $a_m$  and  $b_m$  (which vary on the scale of  $2\pi/\omega_m$ ) so that it makes sense to decompose the waves into rotating triangles

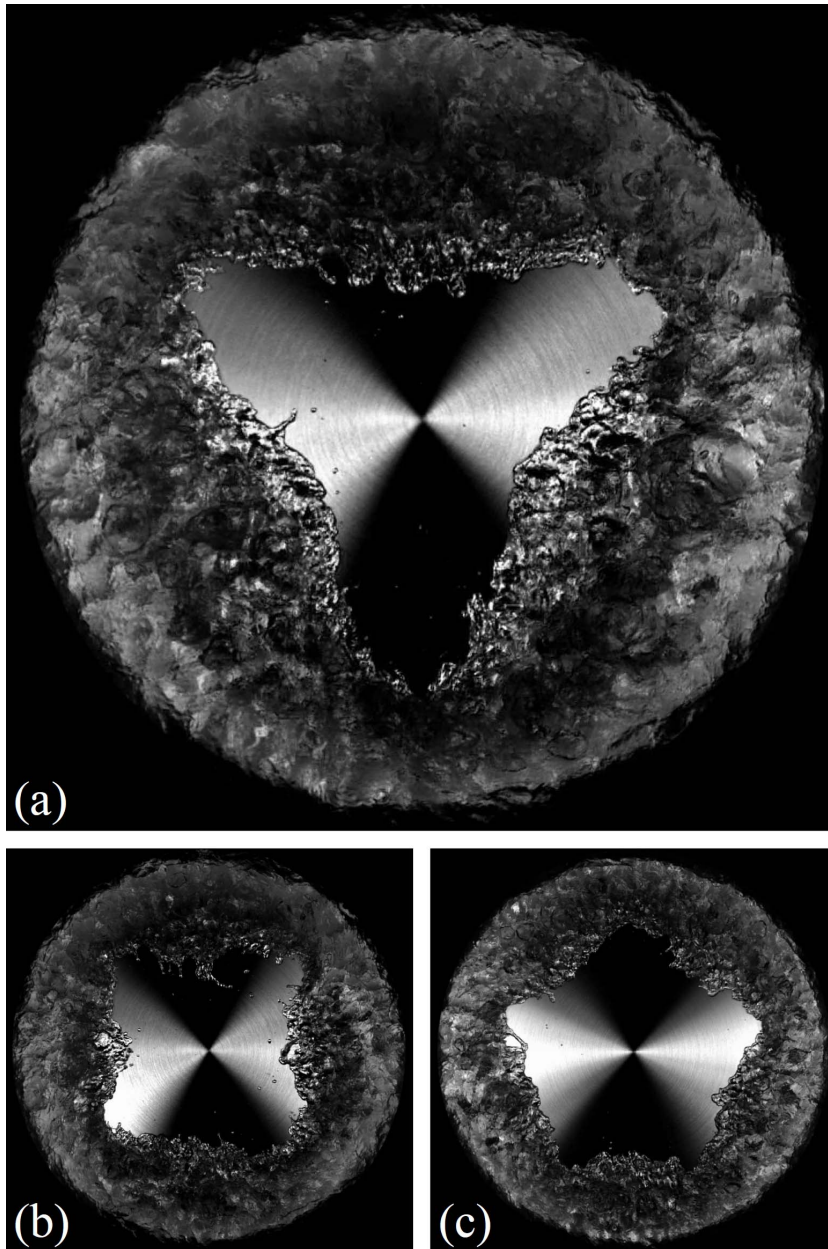


**Figure 7.** Polygons formed by liquid nitrogen in the experiment shown in Figure 6, without the inclined pipe, simply stirring the fluid from rest and using a high-speed camera. The pictures are from [26] and the corresponding video, winner of the Gallery of Fluid Motion in 2018, can be found at <https://gfm.aps.org/meetings/dfd-2018/5b992d40b8ac31610362f452>.

( $m = 3$ ), squares ( $m = 4$ ) etc., and using this decomposition we can quantitatively follow the shape dynamics. In Figure 8a we show the amplitude for each Fourier component  $m = 3-6$  as a function of time, and in Figure 8b-d one can follow the corresponding detected shape.

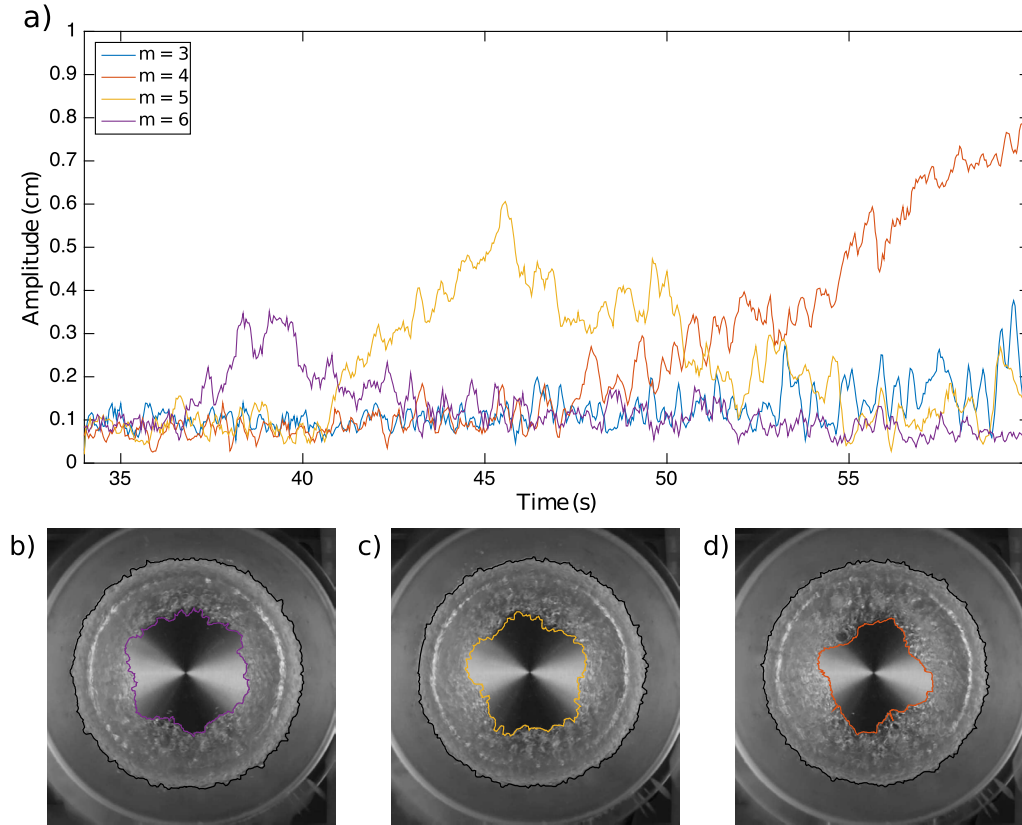


**Figure 8.** Shapes and Fourier amplitudes of rotating polygons in liquid nitrogen. (a) The amplitude of each Fourier component. (b–d) The detected inner and outer fluid surface for  $t = 39$  s,  $t = 45$  s, and  $t = 55$  s.

We can now trace the development of the shapes in time by monitoring the volume of fluid  $V$  and the average value of the shape radius  $\langle \xi \rangle = A_0$  (the zeroth Fourier component) which we use as a proxy for  $\xi$  in (3) to compute the circulation  $\Gamma$ , even though the state might not be circular. In this experiment the volume of fluid  $V$  and the circulation  $\Gamma$  are monotonically decreasing with time, due to evaporation and slowing down, and in fact we also observe a monotonic decrease in the number of corners in the “polygon” observed. This is seen clearly in Figure 8a where we observe an essentially circular state around  $t = 35$  s, a hexagon around  $t = 39$  s, a pentagon around  $t = 45$  s and a square around  $t = 55$  s. Eventually, the volume and circulation get so small that no polygonal shape can be observed. In this example that happens before forming  $m = 3$  or  $m = 2$  shapes.

### 3.2. Wave frequencies and their evolution

In Figure 9a we show an amplitude diagram for another run of the experiment, where the first clearly non-spherical shape  $m = 5$  appeared at  $t \approx 40$  s. In Figure 9b we have plotted the normalized angular frequencies  $\bar{\omega} = \omega / \sqrt{g/R}$  for different  $m$ , where the color shows the value of  $m$  as in Figure 9a. Here solid lines are the detected  $\bar{\omega}_m$  frequencies whereas dotted and dashed lines are the computed gravitational  $\bar{\omega}_{g,m}$  and centrifugal  $\bar{\omega}_{c,m}$  frequencies respectively, calculated from (17) and (18), where the plus-sign is chosen in (17) and the minus sign in (18). The

detected solid lines are bold when the corresponding amplitude is significant. According to the resonance theory [16] described above we then expect to excite a wave when dotted and dashed lines of the same color cross.

First we see that the purple dashed  $\tilde{\omega}_{c,6}$  and purple dotted lines  $\tilde{\omega}_{g,6}$  do not intersect, and, correspondingly, looking at Figure 9a, we see that no hexagon is excited. Returning to Figure 9b following the blue dashed line  $\tilde{\omega}_{c,5}$  and the blue dotted line  $\tilde{\omega}_{g,5}$  we see that these get close around  $t = 40\text{--}55$  s. Now Figure 9a we see that a pentagon is excited in this time interval. Finally, following the green dashed line  $\tilde{\omega}_{c,4}$  and the green dotted line  $\tilde{\omega}_{g,4}$  in Figure 9b we see that these never intersect. However, still a large amplitude square is excited exactly at the centrifugal angular frequency  $\tilde{\omega}_m = \tilde{\omega}_{c,m}$ . Based on these observations one might conjecture that the first excited shape emerging from the circular state, is dictated by resonance between a forward gravitational wave and a backward centrifugal wave in agreement with the theory of Tophøj *et al.* [16], at least if the time scale for this instability is long compared to the life time of the circular state, which is true for our system. However, the next shape changes take place from some fully developed polygon state, which is not close to the circular state, and where therefore the linear stability theory used in [16] would not be valid. We also see that the detected frequency  $\tilde{\omega}_m$  always follows the dispersion of a centrifugal wave alone, and thus that the centrifugal wave is the only survivor after the resonance.

In Figure 9c we show the flow at three different times. Here we have plotted the detected edge (noisy white line), together with the full Fourier decomposition  $\xi(\theta) = \sum_{m=0}^{10} A_m \sin(m\theta - \omega t)$  (smooth white line). The colored lines then show the  $m = 5$ ,  $m = (5 \text{ and } 4)$  and  $m = 4$  Fourier components respectively (always including  $m = 0$  mode). This confirms that the flow is well described by single (nonzero) Fourier components. Even a complicated shape as for  $t = 52.80$  s is well described by a linear combination of Fourier components  $m = 4$  and  $m = 5$ .

### 3.3. Phase diagram

In Figure 10 we show a phase diagram containing multiple runs for the nitrogen experiment where the shape and the weight were simultaneously detected. The grey tongues show the instability regions for the “Tophøj model”, i.e., combinations of  $\tilde{V}$  and  $\tilde{\Gamma}$  where (19) has complex solutions and hence where a backward centrifugal and forward gravitational wave of some wave number  $m$  are in resonance. The numbers at each grey tongue indicate the value of  $m$  for that particular resonance. Note that, as remarked above, the experiments with stationary polygons over a rotating bottom [12] show an entire, compact region of polygons in contrast to the narrow tongues predicted by the theory. Notice in general how hexagons are only formed in the left part near the hexagon-area while triangles are only formed in the right part near the triangle-area. Notice also how experiments initiated to the right of the hexagon-area never excite hexagons as described in relation to Figure 9. Another interesting feature is that the squares seem to distribute all over the phase diagram below  $\tilde{\Gamma} \approx 0.4$  but usually following a pentagon, i.e. they are not excited first. This supports the hypothesis that the first excitation is governed by resonance while following shapes might follow from the previous excitation. This feature can be a consequence of the decrease of  $\tilde{\Gamma}$  and  $\tilde{V}$  due to the setup and would of course be better investigated in a setup where  $\tilde{\Gamma}$  and  $\tilde{V}$  were not changing over time. In Figure 11, we show a more complete phase diagram, where, in Figure 11a we only plot the first discernible polygon appearing in a given experimental run. In Figure 11b we plot our corresponding measurements on the setup described in [19], where stationary rotating polygons appear over a rotating plate as shown in Figure 2b. In principle these two experiments should be very close, but as one can see the deviations from the theory are much larger for the nitrogen experiment. For the water experiment, the theoretical predictions for the  $\tilde{\Gamma}$  corresponding to a given polygon are

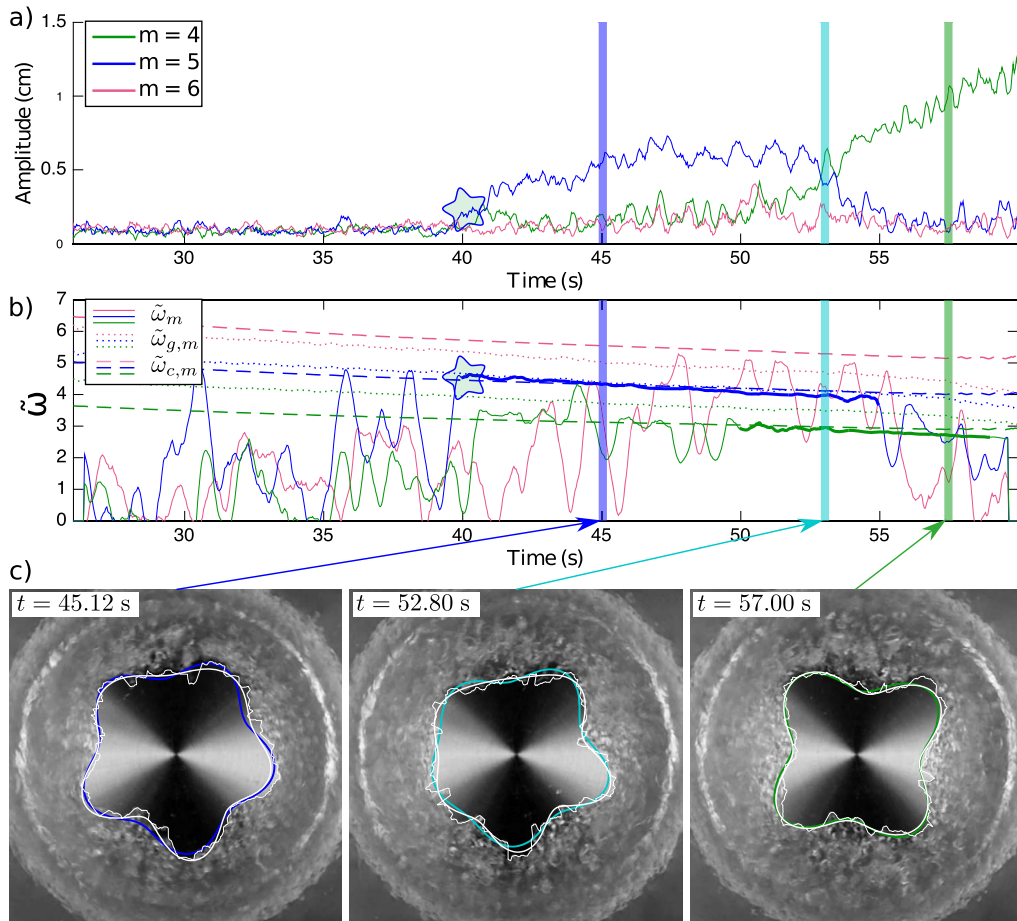


**Figure 9.** Shape and spectral dynamics of the polygon shapes. (a) Fourier amplitudes vs. time. (b) Scaled frequencies  $\tilde{\omega} = \omega/\sqrt{g/R}$  vs. time. The colors follow  $m$  as in (a). Solid lines represents experimental data which are marked bold when the amplitude in (a) is high. Dashed lines are centrifugal backward waves  $\tilde{\omega}_{c,m}$  and dotted lines are gravitational forward waves  $\tilde{\omega}_{g,m}$ . Note how these cross around  $t = 40$  s to  $t = 50$  s where the first wave ( $m = 5$ ) is excited. Note also how the experimental wave (solid) follows the centrifugal waves (dashed). (c) The shape at three different times. White noisy line is the detected edge, white smooth line is sum of Fourier components  $m = 0$  and  $m = 3-6$ , and colored lines are only Fourier component  $m = 0$  with  $m = 5$ ,  $(m = 4) + (m = 5)$  and  $m = 4$  respectively.

consistently lower than the experiments, but actually rather close when we take into account the simplicity of the theory and the fact that the narrow theoretical polygon-tongues should actually fill up the entire region shown. The predictions for the nitrogen experiment Figure 11a correspond best with the experiments for hexagons and pentagons, whereas polygons with fewer corners are further off and the borders between the respective regions seem to be more horizontal than for water. Why this is so, we do not know, but one reason might be that the description of the flow as a line vortex is worse for the nitrogen flow with its strong fluctuations. To test this we show in Figure 12 a comparison of the measured values of  $\tilde{\xi}$  and the predicted (“theoretical”) values. For each state  $\tilde{\xi}$  and  $\tilde{\zeta}$  were determined experimentally. We included only circular states, either



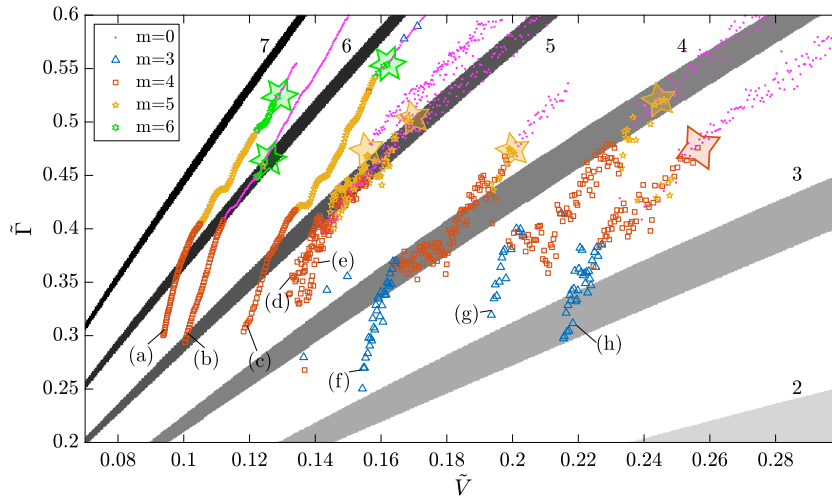


**Figure 10.** Phase diagram for multiple runs of the nitrogen experiment. In each run,  $\tilde{V} = V/(\pi R^3)$  and  $\tilde{\Gamma} = \Gamma/(2\pi\sqrt{gR^3})$  are followed in time and the surface shape is indicated at each time step. The grey tongues show the instability regions for the Tophøj model. The large symbols show the first discernible polygon appearing in a given run.

states that remain circular or the circular state preceding a polygon. For water (filled blue points), the determination of  $\tilde{\zeta}$  is easy, since the cylinder is transparent. For nitrogen (open red circles)  $\tilde{\zeta}$  was determined from the videos taken from above, comparing with the pictures of an empty pot equipped with a vertical measuring rod at the rim. We then used this experimental  $\tilde{\zeta}$  in (15) and (16), i.e.,

$$\tilde{\zeta} = \frac{\tilde{V}(1 - \tilde{\xi}^2)}{1 - \tilde{\xi}^2 + 2\tilde{\xi}^2 \ln(\tilde{\xi})} \quad (23)$$

to determine a “theoretical”  $\tilde{\xi}$ . As seen in Figure 12, the experimental and theoretical values of  $\tilde{\zeta}$  for water are extremely close, since the blue points are very close to the diagonal. For nitrogen, the correspondence is not that close. The open red circles are more strongly scattered, as we would have expected since the determination of  $\tilde{\zeta}$  is much harder in this case, but they also lie above the diagonal, i.e., have  $\tilde{\xi}_{\text{th}} > \tilde{\xi}_{\text{exp}}$ , implying a systematic deviation from the line vortex flow, perhaps due to the strong turbulence.

#### 4. Conclusions

We have described a quite surprising experiment, where spontaneous large scale ordering takes place despite strong disorder at the small scales in the form of drop-ejection and turbulent eddies. We have compared the system to a theory based on potential perturbations on a laminar potential vortex flow, and we find some correspondence, but also large deviations. The system contains some interesting features, e.g., displaying a “critical line” separating subcritical flow at the rim from supercritical flow at the center. Such a line is the distinguishing feature, which determines whether a given frequency (as in Figure 5) will give rise to an instability or not. A feature, which is *not* captured by the theory, however, is the fact that one of these modes, the centrifugal wave near the center, becomes totally dominant with an amplitude orders of magnitude larger than the gravitation one. Correspondingly, the system displays a kind of one-way coupling: a perturbation near the rime seems to propagate readily toward the center, whereas

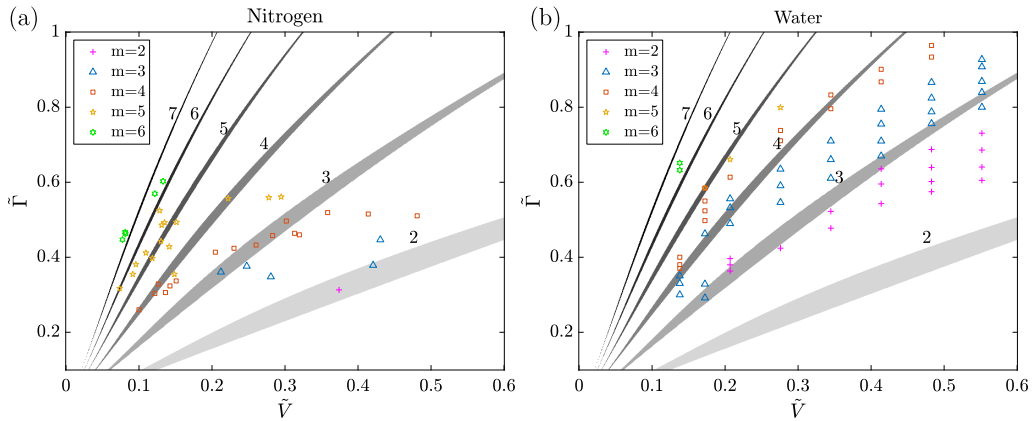


**Figure 11.** Phase diagram for the nitrogen experiment and for water over a rotating bottom. (a) For each run of the nitrogen experiment, only the first discernible polygon is marked. The determination of  $\tilde{r}$  is made through the value of  $\tilde{\xi}$  in the circular state preceding the polygon using (15). (b) The corresponding phase diagram for the water experiment, described in [19], where stationary rotating polygons appear. Here, the determination of  $\tilde{r}$  is made through the value of the exterior height  $\tilde{\zeta}$  and rest-height  $\tilde{V}$  using (15) and (16) to eliminate  $\tilde{\xi}$ . In the water experiment the cylinder is transparent and it is easy to measure the height at the rim.

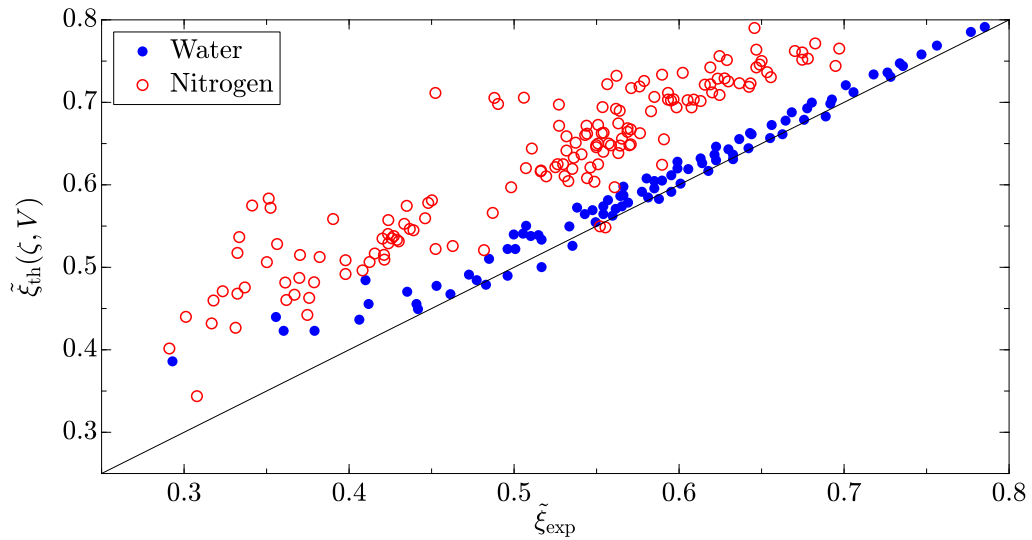


**Figure 12.** Experimental test of the “line vortex” approximation (1)–(3) by comparing the experimentally determined value of  $\tilde{\xi}$  with a theoretical value determined through a measurement of  $\tilde{\zeta}$  as explained in the text. The blue points are the results for water and the open red circles are for the nitrogen experiment. Only values of  $\zeta$  larger than 20 mm have been kept, due to the difficulty of this measurement for small  $\zeta$ .

on at the rim only perturbs the rim very weakly. Finally, the agreement with theory is a lot better for the (stationary) water experiment than for the nitrogen experiment. This goes also for the flow structure of the circular states (i.e., the base-flow), where the deviations from the potential

vortex flow is larger for the nitrogen experiment, maybe because of the large eddy-viscosity. In conclusion, we cannot help asking ourselves: What would Yves have said?

## Acknowledgements

We are extremely grateful to Laust Tophøj, Martijn van der Ouderaa, Erik Hansen, Mette Høst and Asbjørn Lauritsen for invaluable help in the design and lighting of the experiment and to Jerome Mougél for useful advice. The research leading to these results has received funding from the People Programme (Marie Curie Actions) of the European Union's Seventh Framework Programme (FP7/2007-2013) under REA grant agreement no. 609405 (COFUND Postdoc DTU).

## Appendix A. Details of the experiment

In Table 1 we describe some of the important parameters for our experiments.

**Table 1.** Experimental setup information

Fixed experiment parameter	Value
Weight model	Kern DE60K1DL
Weight resolution	1 g
Weight equilibrium time	2 s
Camera ISO	500
Camera aperture	F6.3
Frame rate	50 f/s
Shutter speed	1/400 s
Distance from camera to bottom of pot	~40 cm
Number of spotlights	2
Radius of pot	10 cm
Inclination angle of pipe	14°–16°
Length of pipe	1.25 m
Initial temperature of surrounding water bath	60 °C

## References

- [1] Y. Couder, "Submillimeter cyclotron resonance in tellurium", *Phys. Rev. Lett.* **22** (1969), p. 890-892.
- [2] E. Fort, A. Eddi, J. Moukhtar, A. Boudaoud, Y. Couder, "Path-memory induced quantization of classical orbits", *Proc. Natl Acad. Sci. USA* **107** (2010), no. 41, p. 17515-17520.
- [3] Y. Couder, "The observation of a shear-flow instability in a rotating system with a soap membrane", *C. R. Acad. Sci. Ser. II* **293** (1981), no. 1, p. 1.
- [4] A. Arneodo, F. Argoul, Y. Couder, M. Rabaud, "Diffusion controlled growth phenomena: from smooth interfaces to fractal structures", *NATO ASI Ser. B* **276** (1991), no. 297, p. 1.
- [5] Y. Couder, L. Pauchard, C. Allain, M. Adda-Bedia, S. Douady, "The leaf venation as formed in a tensorial field", *Eur. Phys. J. B* **28** (2002), p. 135-138.
- [6] S. Bohn, B. Andreotti, S. Douady, J. Munzinger, Y. Couder, "Constitutive property of the local organization of leaf venation networks", *Phys. Rev. E* **65** (2002), 061914.
- [7] O. Hamant *et al.*, "Developmental patterning by mechanical signals in arabidopsis", *Science* **322** (2008), p. 1650.
- [8] K. H. Jensen, E. Rio, R. Hansen, C. Clanet, T. Bohr, "Osmotically driven pipe flows and their relation to sugar transport in plants", *J. Fluid Mech.* **636** (2009), p. 371.
- [9] S. Perrard, Y. Couder, E. Fort, L. Limat, "Leidenfrost levitated liquid tori", *Europhys. Lett.* **100** (1969), 54006.
- [10] C. Ellegaard, A. E. Hansen, A. Haaning, A. Marcussen, T. Bohr, J. Hansen, S. Watanabe, "Creating corners in kitchen sink flows", *Nature* **392** (1998), p. 767-768.

- [11] G. H. Vatistas, "A note on liquid vortex sloshing and Kelvin's equilibria", *J. Fluid Mech.* **217** (1990), p. 241-248.
- [12] T. R. N. Jansson, M. P. Haspang, K. H. Jensen, P. Hersen, T. Bohr, "Polygons on a rotating fluid surface", *Phys. Rev. Lett.* **96** (2006), 174502.
- [13] R. Bergman, L. Tophøj, T. A. M. Homan, P. Hersen, A. Andersen, T. Bohr, "Polygon formation and surface flow on a rotating fluid surface", *J. Fluid Mech.* **679** (2011), p. 415-431.
- [14] J. Bush, J. Aristoff, A. E. Hosoi, "Model for polygonal hydraulic jumps", *J. Fluid Mech.* **558** (2016), p. 33.
- [15] E. A. Martens, S. Watanabe, T. Bohr, "Model for polygonal hydraulic jumps", *Phys. Rev. E* **85** (2012), 036316.
- [16] L. Tophøj, J. Mougel, T. Bohr, D. Fabre, "Rotating polygon instability of a swirling free surface flow", *Phys. Rev. Lett.* **110** (2013), no. 19, 194502.
- [17] J. Mougel, D. Fabre, L. Lacaze, T. Bohr, "On the instabilities of a potential vortex with a free surface", *J. Fluid Mech.* **824** (2017), no. 19, p. 230-264.
- [18] G. H. Vatistas, H. A. Abderrahmane, M. H. K. Siddiqui, "Experimental confirmation of Kelvin's equilibria", *Phys. Rev. Lett.* **100** (2008), 174503.
- [19] B. Bach, E. C. Linnartz, M. H. Vested, A. Andersen, T. Bohr, "From Newton's bucket to rotating polygons: experiments on surface instabilities in swirling flows", *J. Fluid Mech.* **759** (2014), p. 386-403.
- [20] L. Tophøj, T. Bohr, "Stationary ideal flow on a free surface of a given shape", *J. Fluid Mech.* **721** (2013), p. 28-45.
- [21] J. Mougel, D. Fabre, L. Lacaze, "Waves in Newton's bucket", *J. Fluid Mech.* **783** (2015), p. 211-250.
- [22] R. Cairns, "The role of negative energy waves in some instabilities of parallel flows", *J. Fluid Mech.* **92** (1979), p. 1.
- [23] K. Iga, S. Yokota, S. Watanabe, T. Ikeda, H. Niino, N. Misawa, "Various phenomena on a water vortex in a cylindrical tank over a rotating bottom", *Fluid Dyn. Res.* **46** (2014), 031409.
- [24] M. Iima, Y. Tasaka, "Dynamics of flow structures and surface shapes in the surface switching of rotating fluid", *J. Fluid Mech.* **789** (2016), p. 402-424.
- [25] R. Yellin-Bergovoy, E. Heifetz, O. M. Umurhan, "Physical mechanism of centrifugal-gravity wave resonant instability in azimuthally symmetric swirling flows", *Phys. Rev. Fluids* **2** (2017), 104801.
- [26] A. Duchesne, T. Bohr, B. Bohr, L. Tophøj, "Nitrogen swirl: creating rotating polygons in a boiling liquid", *Phys. Rev. Fluids* **4** (2019), 100507.